British Columbia Geological Survey
Geological Fieldwork 1989

TEMPERATURE AND COMPOSITION OF FLUIDS IN THE BASE METAL RICH SILBAK PREMIER Ag-Au DEPOSIT, STEWART, B.C. (104B/1)

By Dean McDonald
University of Western Ontario

KEYWORDS: Economic geology, Silbak Premier, epithermal, paragenesis, fluid inclusions, homogenization temperatures, salinities, Raman spectrometry, deposit models.

INTRODUCTION

The Silbak Premier mine is in northwest British Columbia, 21 kilometres north of Stewart (Figure 2-12-1), on the east side of the Salmon River Valley. The original discovery of a high-grade vein in 1910 culminated in an underground mine that from 1918 to 1953 produced 4.3 million tonnes of ore grading 14.6 grams gold and 304 grams silver per tonne from sulphide-bearing stockwork veins and breccia zones. Current open pit reserves are 5.9 million tonnes grading 80.23 grams per tonne silver and 2.16 grams per tonne gold (Randall, 1988).

Chemical composition of ore-forming fluids has been estimated by measuring the temperature of homogenization and freezing point depression of fluid inclusions; mass spectral analysis of gaseous species using a Raman spectrometer; and microprobe x-ray maps of precipitates from fluid inclusions to define nonvolatile components. These fluid inclusions are in quartz which can be reliably placed in the paragenetic sequence. The change in temperature and chemical composition of fluids before, during, and after ore deposition are used to interpret chemical constraints on gold and base metal deposition. These constraints assist development of an exploration model.

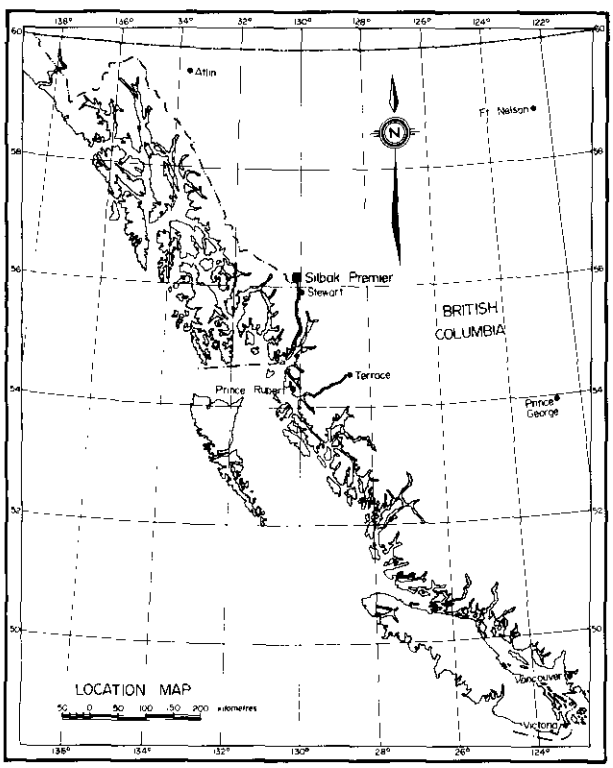

Figure 2-12-1. Location of Silbak Premier deposit near Stewart, B.C.

REGIONAL GEOLOGY

The Silbak Premier deposit is at the west margin of the Intermontane Belt, adjacent to the Coast Belt. It is hosted by north-northwest-trending volcanic rocks of the Hazelton Group that are unconformably overlain by sedimentary rocks of the Bowser Group to the east (Alldrick, 1985, 1987). The Hazelton Group comprises Late Triassic to Early Jurassic andesite flows, breccias and tuffs overlain by Early Jurassic dacite lapilli tuffs, dacite flows and volcaniclastic rocks. Rhyolite breccia and tuff are a regional marker horizon at the top of the Hazelton Group (Brown, 1987). Three intrusive episodes are represented by porphyritic dacite of the Early Jurassic Texas Creek plutonic suite, Eocene Hyder quartz monzonite and granodiorite, and Oligocene to Miocene biotite lamprophyre dikes.

The regional structure is a north-northwest-striking system of open to tight folds with moderate to steeply dipping west-southwest cleavage. Northerly trending, right-lateral strike-slip faults segment regional stratigraphy. Metamorphic grade is lower greenschist facies with a thermal peak of 330°C (Alldrick *et al.*, 1987).

GEOLOGY OF SILBAK PREMIER DEPOSIT

The Silbak Premier deposit consists of sulphide-bearing, parallel and stockwork veins and breccia zones marginal to and crosscutting irregular to tabular plugs and dikes of Jurassic potassium feldspar porphyritic dacite. Discrete and conjugate merging lobes of dacite intrude or are conformable with andesite flows, breccias and tuffs and dacite flows of Late Triassic to Early Jurassic age (Figure 2-12-2 and 2-12-3). Eocene granodiorite, quartz monzonite and microdiorite dikes traverse andesite-dacite volcanic and intrusive rocks.

Layering in dacite flows has a north to northwest strike with a variable westward dip. Cleavage developed during the first fold generation has a northerly strike with a variable dip to the west. At the deposit, this broad open fold is an asymmetric syncline with a steep east limb. The second foliation is a spaced fracture cleavage which strikes east and

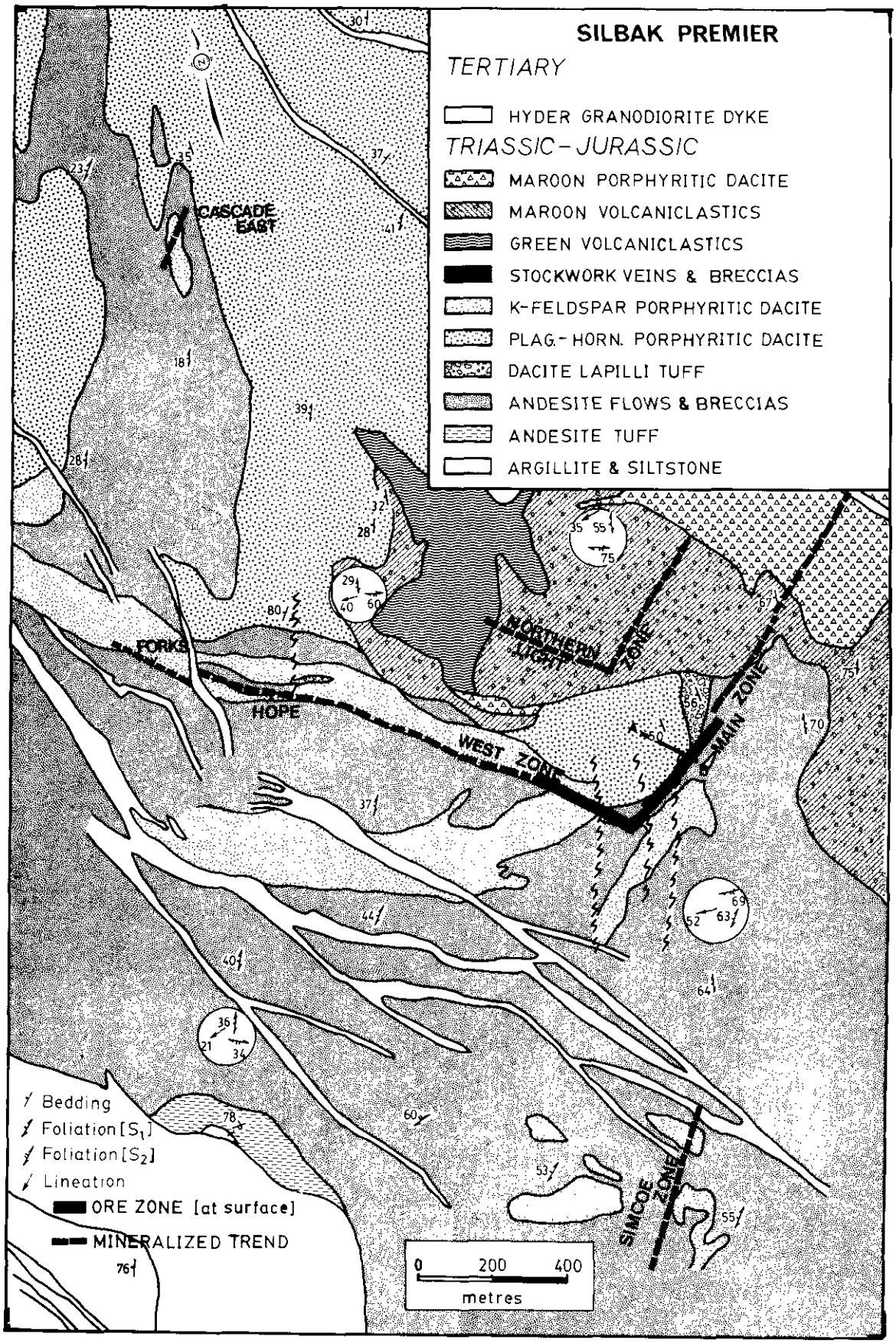

Figure 2-12-2. Surface map of the Silbak Premier deposit with superimposed surface trends of stockwork veins and breccias. Cross-section 2340 N (Figure 2-12-3) is defined by line A-B through the Main zone. Portions modified from Brown (1987).

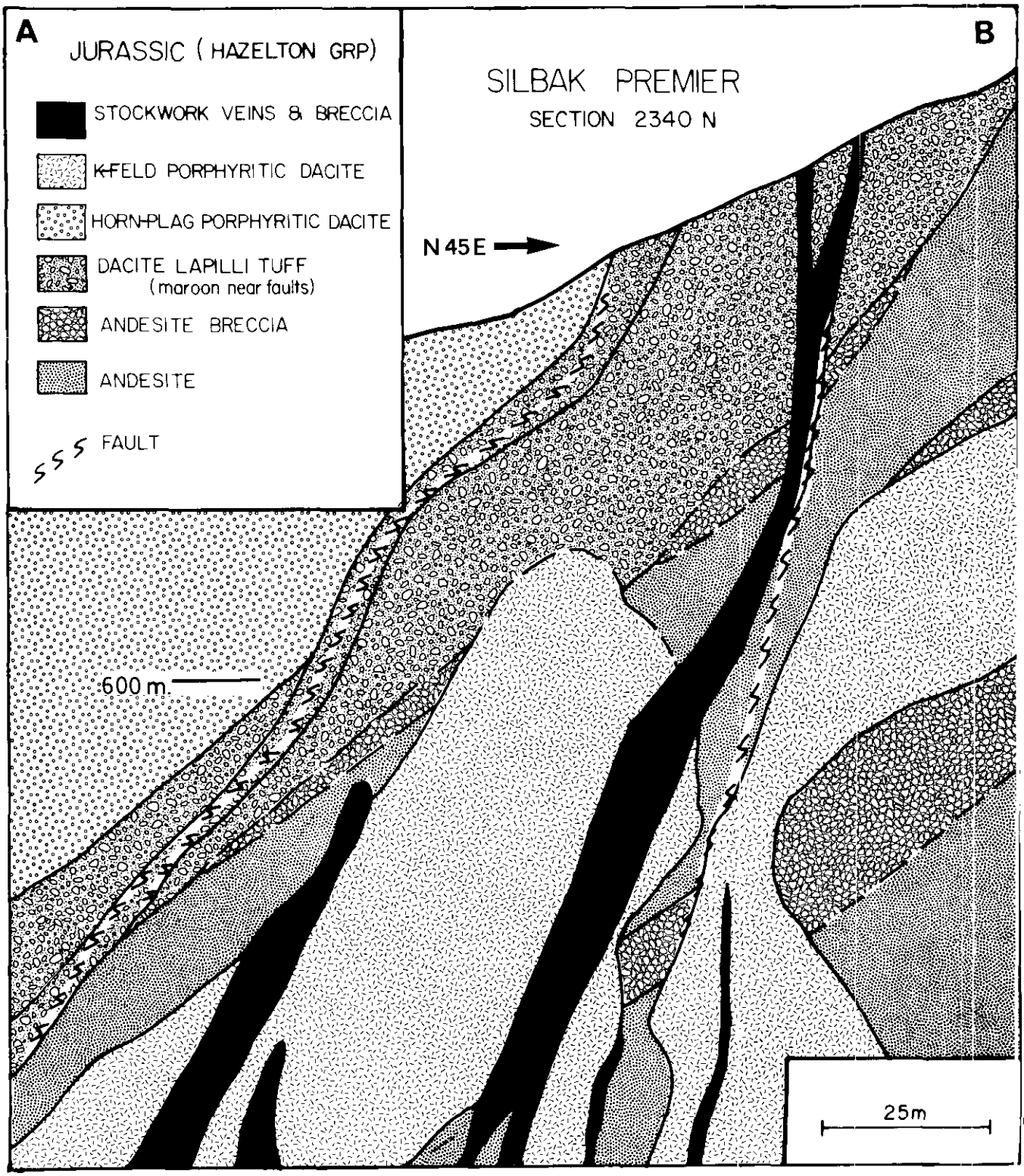

Figure 2-12-3. Geological cross-section 2340 N. Sharply defined veins in stockworks and matrix-to-breccia contain metallic mineral assemblages and follow a number of subparallel trends within and marginal to a potassium feldspar porphyritic dacite. The porpyritic dacite and metal-bearing veins and breccias exhibit both conformable and crosscutting relationships with andesite and dacite country rocks of Jurassic age.

dips south. Subsequent conjugate faults are the locus for porphyritic dacite intrusions, breccias and stockwork veins.

Breccias and veins formed before, during and after ore deposition and are referred to as early, middle and late-stages, respectively. Early-stage breccia is a crackle or *in situ* breccia occuring as a 5 to 15-metre zone of siliceous, rounded to angular andesite fragments enclosed in a quartz, calcite and pyrite matrix. These breccia zones are both coeval with and subsequent to the intrusion of porphyritic dacite and form within andesite peripheral to it. Early-stage veins are primarily banded quartz and chlorite with pyrite accummulations along the margins. They are subparallel, and crosscut early-stage crackle breccia, but are cut by middle-stage stockwork veins.

Middle-stage stockwork veins and matrix to the breccia contain most of the metallic minerals and the greatest amount of silver and gold. They have distinct precious and base metal rich mineral assemblages where base metal abundances increase and precious metals decrease with depth. Orthogonal fractures are infilled with quartz, pyrite and minor amounts of electrum, polybasite, pyrargyrite, argentite and native silver. Late, coarse-grained quartz-chlorite veins occupy vertical and horizontal fractures and cut stockwork veins in en echelon pattern.

Early-stage breccia with propylitic alteration minerals chlorite, pyrite, calcite and sericite developed within andesite along the upper margins of the porphyritic dacite. Middle-stage propylitic alteration is overprinted by potassic alteration minerals potassium feldspar and sericite in the wallrock adjacent to veins and breccias. Narrow envelopes of propylitic alteration occur on the margins of late-stage veins.

Both precious and base metal rich veins and mineralized breccia matrix show a paragenetic sequence from sulphide-rich minerals to sulphosalts and native minerals (McDonald, 1988). In both types of veins, pyrite is earliest and is coincident with quartz. Subsequent sulphide and sulphosalt minerals occur with quartz and later potassium feldspar.

STUDY OF FLUID INCLUSIONS

DESCRIPTION

Fluid inclusions are small, generally microsopic, volumes of fluid trapped in irregularities within crystals. Although typically trapped as a homogeneous fluid at the temperature of growth, they are normally multiphase (solid, liquid, vapour) at room temperature. The sealing off of such irregularities in crystals may occur during the growth of the surrounding crystal to make primary fluid inclusions, or by recrystallization along fractures at a later time forming pseudosecondary or secondary inclusions (Roedder, 1984).

There are two optically distinct varieties of quartz in all veins examined: grey to milky translucent quartz and transparent quartz which either engulfs or occurs along microfractures in milky quartz. Milky quartz is usually turbid and has many isolated clusters of inclusions and tiny grit-like particles without birefringence or crystal form. The minute size and high density of inclusions in milky quartz make them unsuitable for study.

Fluid inclusions in clear quartz typically have a liquid phase and vapour bubble. Daughter minerals, halite and sylvite, are noticeably absent. Primary, pseudosecondary and secondary inclusions are discriminated by size, shape and distribution with respect to fractures in quartz.

TYPES OF INCLUSIONS

Primary inclusions are identified by their solitary location unrelated to fractures (Plate 2-12-1A) or in zones parallel to and within zoned crystal growths (Plates 2-12-1B and 2-12-1C). Two populations of primary fluid inclusions are present:

Type 1 primary inclusions are elliptical to irregularly shaped, 5 to 15 microns in diameter, and in places necked. These two-phase, liquid-vapour inclusions account for 90 per cent of primary inclusions with relatively constant 20 to 30 volume per cent vapour and no daughter crystals.

Type 2 liquid-vapour, primary inclusions are rare, rounded to elliptical and 15 to 20 microns in diameter (Plate 2-12-1D). The vapour to liquid volumetric ratios for Type 2 inclusions are fairly uniform, with the vapour phase commonly occupying less than 20 per cent of the inclusion volume. Type 2 inclusions are most common in vuggy quartz and late-stage veins. Inclusions in both base and precious metal, middle-stage veins have similar degrees of fill, however, late-stage veins appear to have more volume of fill.

Pseudosecondary inclusions are planes of inclusions that traverse growth zones, but do not cross grain boundaries (Plate 2-12-1E). Dense clusters of fluid inclusions are called pseudosecondary because one cannot be certain they are primary. Pseudosecondary inclusions closely resemble primary inclusions in size, but are commonly necked. The volume of liquid and vapour is variable from 20 to 35 per cent. No daughter crystals have been identified.

Secondary inclusions occur in planar arrays that traverse growth zones (Plate 2-12-1F), tend to be 1 to 5 microns in diameter, and elliptical to flattened. They are more common than primary inclusions and normally occur along fracture planes. A few secondary inclusions are liquid only, however, volume of gas bubbles typically varies from 10 to 30 per cent.

HOMOGENIZATION TEMPERATURES

Fluid inclusions were studied by standard heating and freezing techniques on a Th 600 Linkam gas-flow heating and freezing stage (MacDonald and Spooner, 1981). The stage was calibrated using small samples of reagent-grade compounds with known melting points for the temperature range of $-30°$ to 350°C. Homogenization measurements were assessed with melting point standards and were reproducable within 1°C for temperatures in the range $-20°$ to 250°C and as much as 3°C for higher temperatures. This study is based on 410 measurements on 21 samples from three different phases of veining (Table 2-12-1, Figure 2-12-4).

Homogenization temperatures of primary inclusions in early-stage veins ranged from 179° to 240°C with an average of 204.6°C. Primary inclusions in quartz from precious metal rich, middle-stage veins homogenize from 187° to 287°C and average 225.4°C. Inclusions from base metal rich, middle-stage veins have slightly higher homogenization temperatures that range from 180° to 292°C and average 228.8°C.

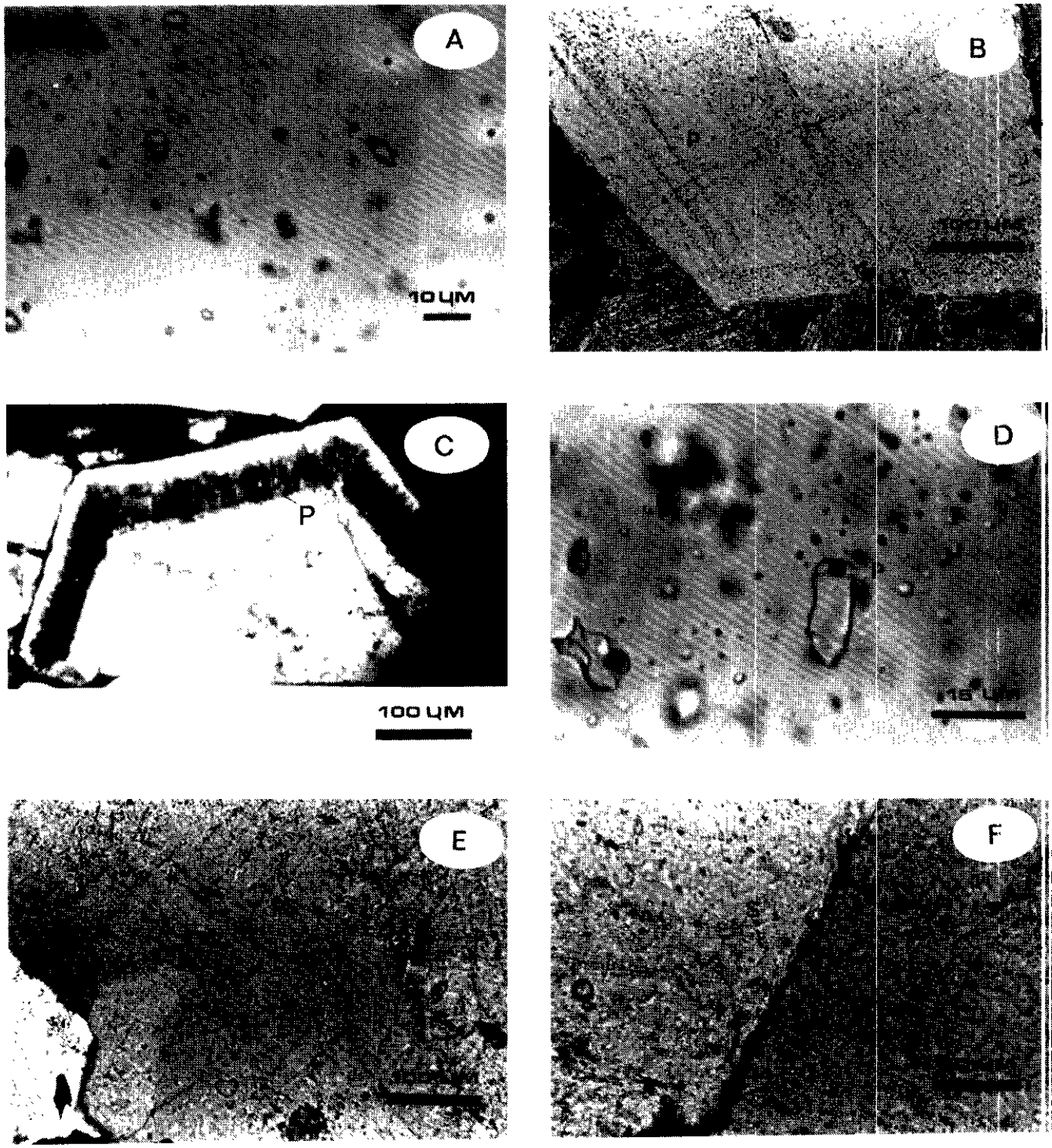

Plate 2-12-1.

A. Photomicrograph of a two-phase primary inclusion (P); water solution plus vapour bubble. Polished section SP-221.

B. Photomicrograph of milky quartz crystal cut perpendicular to the C-axis. Crystal growth was not continuous, but episodic, as evidenced by the band of primary inclusions (P). Polished section SP-114-A.

C. Photomicrograph of concentric band of primary inclusions (P) in the interior of a hexagonal quartz crystal. Polished section SP-47-U.

D. Photomicrograph of Type 2 aqueous primary inclusions (P) with vapour bubbles. Polished section SP-10.

E. Photomicrograph of intersecting pseudosecondary inclusions (PS). The planar array of inclusions does not cross grain boundaries. Polished section SP-80.

F. Photomicrograph, taken with partly crossed polars, of planes of secondary inclusions in quartz from gold-quartz veins. Note that many of the planes crosscut grain boundaries, outlining former throughgoing fractures. Polished section SP-181.

Type 2 primary inclusions have similar homogenization temperature ranges as Type 1 inclusions in all vein stages. Homogenization temperatures for pseudosecondary inclusions in each stage of veining are typically 10° to 20°C lower than their primary equivalent. Homogenization temperatures from secondary inclusions are similar in all stages of mineralization and range from 140° to 216°C, averaging 167°C.

Freeing Point Depression Temperature

The salinity of fluid inclusions is estimated from depression of the freezing point of ice using a gas-cooled freezing stage. The results are expressed as equivalent weight per cent NaCl, because NaCl is found to be the major salt component in the inclusions. Freezing point determinations from each vein stage (Table 2-12-2 and Figure 2-12-5) were measured on the same fluid inclusions used for heating studies.

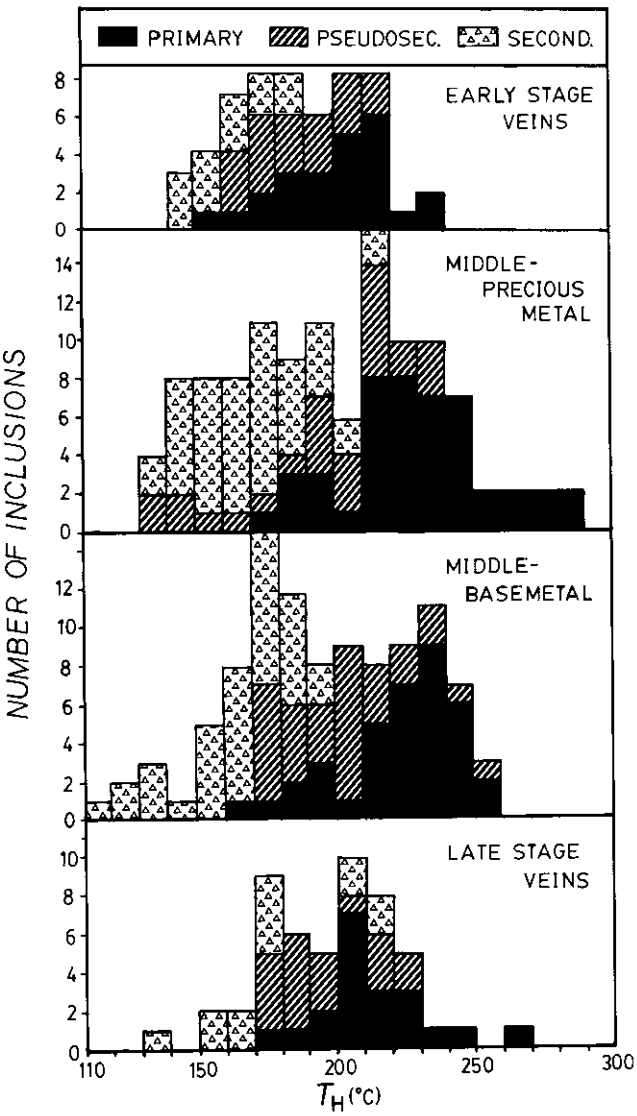

Figure 2-12-4. Histogram of homogenization temperatures for fluid inclusions. Dark areas are primary inclusions in quartz, banded areas are pseudosecondary and stippled triangled areas are secondary. Both early and late-stage veins are barren of sulphides.

TABLE 2-12-1
HOMOGENIZATION TEMPERATURES OF FLUID INCLUSIONS

SAMPLE #	Location	Elevation	Stage	Type	No. Inc	Range Temp	Mean Temp
SP-165	DH 85-69	615.76	I	P	10	182-240	209.1
			I	PS	8	162-214	186.3
			I	S	4	151-189	165.2
SP-166A	DH 87-248	652.42	I	P	9	179-220	199.6
			I	PS	9	168-211	185.7
			I	S	5	147-181	165.8
SP-50S	Surface	664.66	II-P.M.	P	8	207-227	218.2
			II-P.M.	PS	7	195-246	224.7
			II-P.M.	S	5	156-216	178.6
SP-97S	Surface	675.76	II-P.M.	P	8	189-216	204.9
			II-P.M.	PS	5	176-198	182.8
			II-P.M.	S	5	156-216	184.2
SP-229	DH 86-79	600.04	II-P.M.	P	11	198-228	212.4
			II-P.M.	PS	7	186-221	201.5
			II-P.M.	S	5	152-204	178.8
SP-59U	110 Level	581.82	II-P.M.	P	10	200-235	221.4
			II-P.M.	PS	6	146-191	163.7
			II-P.M.	S	4	164-191	177.1
SP-51U	110 Level	583.33	II-P.M.	P	8	229-287	242.6
			II-P.M.	PS	6	205-225	215.4
			II-P.M.	S	5	163-211	177.4
SP-207A	2-Level	530.31	II-P.M.	P	8	212-241	229.1
			II-P.M.	PS	5	194-218	206.3
			II-P.M.	S	4	144-166	155.5
SP-47A	2-Level	530.45	II-P.M.	P	8	217-243	231.4
			II-P.M.	PS	5	201-231	216.9
			II-P.M.	S	6	149-194	167.1
SP-204A	3-Level	478.79	II-P.M.	P	10	206-263	240.6
			II-P.M.	PS	6	206-242	221.2
			II-P.M.	S	4	179-205	188.8
SP-213A	5-Level	312.12	II-P.M.	P	11	187-256	218.4
			II-P.M.	PS	6	163-211	192.8
			II-P.M.	S	5	109-141	152.2
SP-5U	6-Level	234.24	II-P.M.	P	9	193-273	238.1
			II-P.M.	PS	6	178-215	193.9
			II-P.M.	S	6	138-167	149.2
SP-136A	Surface	666.67	II-B.M.	P	9	196-241	219.6
			II-B.M.	PS	6	187-228	205.3
			II-B.M.	S	5	147-182	169.2
SP-158	DH 85-74	633.34	II-B.M.	P	10	187-231	214.6
			II-B.M.	PS	6	156-193	176.4
			II-B.M.	S	5	132-178	155.5
SP-48A	DH 86-114	564.24	II-B.M.	P	11	198-244	228.7
			II-B.M.	PS	7	184-220	202.4
			II-B.M.	S	5	153-204	179.2
SP-203A	3-Level	478.79	II-B.M.	P	10	217-271	244.6
			II-B.M.	PS	6	173-237	205.9
			II-B.M.	S	5	142-171	155.3
SP-214A	5-Level	312.12	II-B.M.	P	9	212-292	249.3
			II-B.M.	PS	7	187-227	199.8
			II-B.M.	S	6	148-210	172.3
SP-200A	6-Level	234.24	II-B.M.	P	10	180-242	217.2
			II-B.M.	PS	9	182-207	189.1
			II-B.M.	S	5	112-182	155.2
SP-118	DH 84-35	647.58	III	P	10	179-219	208.4
			III	PS	5	174-217	206.6
			III	S	4	141-171	154.5
SP-14A	DH 87-255	667.58	III	P	9	184-220	204.1
			III	PS	7	182-201	186.1
			III	S	6	151-206	168.4
SP-112A	DH 87-235	602.73	III	P	9	197-236	213.1
			III	PS	8	176-212	206.5
			III	S	5	140-179	164.4

* I— EARLY-STAGE
II— MIDDLE-STAGE
BM— BASE METAL RICH
PM— PRECIOUS METAL RICH
III— LATE-STAGE

The melting point of ice in H_2O-dominant inclusions from early-stage veins range from 0.0° to -0.3°C, corresponding to salinities of about 0 to 2 equivalent weight per cent NaCl. Inclusions from precious metal rich, middle-stage veins have salinities ranging from 0.5 to 3.0. Salinities of base metal rich, middle-stage veins are slightly greater than the precious metal rich, ranging from 0.4 to 4.5. Late-stage veins have salinities from 0 to 1.5 NaCl. Type 1 inclusions have slightly greater salinities than Type 2 inclusions.

During freezing of inclusions, no unusual solid phases such as CO_2 hydrate were observed. Because the most abundant solute in the inclusions is normally NaCl, the commonest hydrate observed is hydrohalite ($NaCl \cdot 2H_2O$) The low Tm_{ICE} values indicate the presence of minor hydrohalites in the inclusions.

Laser-Excited Raman Microprobe Analysis

The laser-excited Raman spectrometer is a generally non-destructive, *in situ*, semiquantitative analytical technique in which the laser beam is focused on a doubly polished wafer to give pinpoint analysis of individual fluid inclusions (Delhaye and Dhamelicourt, 1975; Rosasco *et al.*, 1975).

The laser-excited Raman Spectrometer at Surface Science Western is a Dilor OMARS 89, equipped with an optical multichannel analyzer. As a light beam passes through a medium the vibration spectra are used to characterize the nature and structure of compounds in individual inclusions. A small part of the photon scattering that results from this interaction is inelastic, Raman scattering, and gives rise to radiation of displaced frequencies, or wavenumbers, that are characteristic of the scattering substance.

Inclusions from all three periods of veining are predominantly H_2O with minor, variable CO_2 (Figure 2-12-6). Inclusions from middle-stage veins also have trace abundances of N_2 and CO, however, high H_2O background makes them difficult to detect. The abundances of volatile components for each vein type are given in Table 2-12-3.

TABLE 2-12-2
FLUID INCLUSION SALINITIES

SAMPLE #	Location	Elevation	Stage	Type	No. Inc	Saln. Range	Mean Saln.
SP-165	DH 85-69	615.76	I	P	4	0.1-0.9	0.55
SP-166A	DH 87-248	652.42	I	P	4	0.3-1.5	0.65
SP-50S	Surface	664.66	II-P.M.	P	5	0.8-2.2	1.5
SP-59U	110 Level	581.82	II-P.M.	P	5	0.6-2.2	1.2
SP-207A	2-Level	530.31	II-P.M.	P	5	1.0-3.0	1.45
SP-204A	3-Level	478.79	II-P.M.	P	4	1.0-2.8	1.75
SP-136A	Surface	666.67	II-B.M.	P	5	1.0-3.5	2.1
SP-203A	3-Level	478.79	II-B.M.	P	5	0.8-3.0	2.05
SP-214A	5-Level	312.12	II-B.M.	P	4	1.2-4.4	2.3
SP-200A	6-Level	234.24	II-B.M.	P	5	1.5-4.1	2.4
SP-118	DH 84-35	647.58	III	P	4	0.2-0.8	0.6
SP-112A	DH 87-235	602.73	III	P	4	0.4-1.4	0.75

* I— EARLY-STAGE
II— MIDDLE-STAGE
BM— BASE METAL RICH
PM— PRECIOUS METAL RICH
III— LATE-STAGE

The ability to estimate mole fractions of species in a multicomponent fluid inclusion is based on theoretical calculations (Wopenka and Pasteris, 1986, 1987). Taking the intensity calibration of the spectrometer into acccount, these formulae reduce to the expression:

$$Xi = (A_i/\sigma_i f_i)/(\Sigma A_i/\sigma_i f_i)$$

where: A_i = average area of the Raman peak measured by *planimeter, multiplied by the intensity* (counts sec^{-1});

i = effective relative cross-section of Raman scattering; and,

f_i = instrument correction factor.

In practice one makes several simplifying assumptions and uses the area of the Raman peaks and the scattering cross-sections, a measure of the scattering efficiency of a particular vibrational mode for those species, to calculate their relative

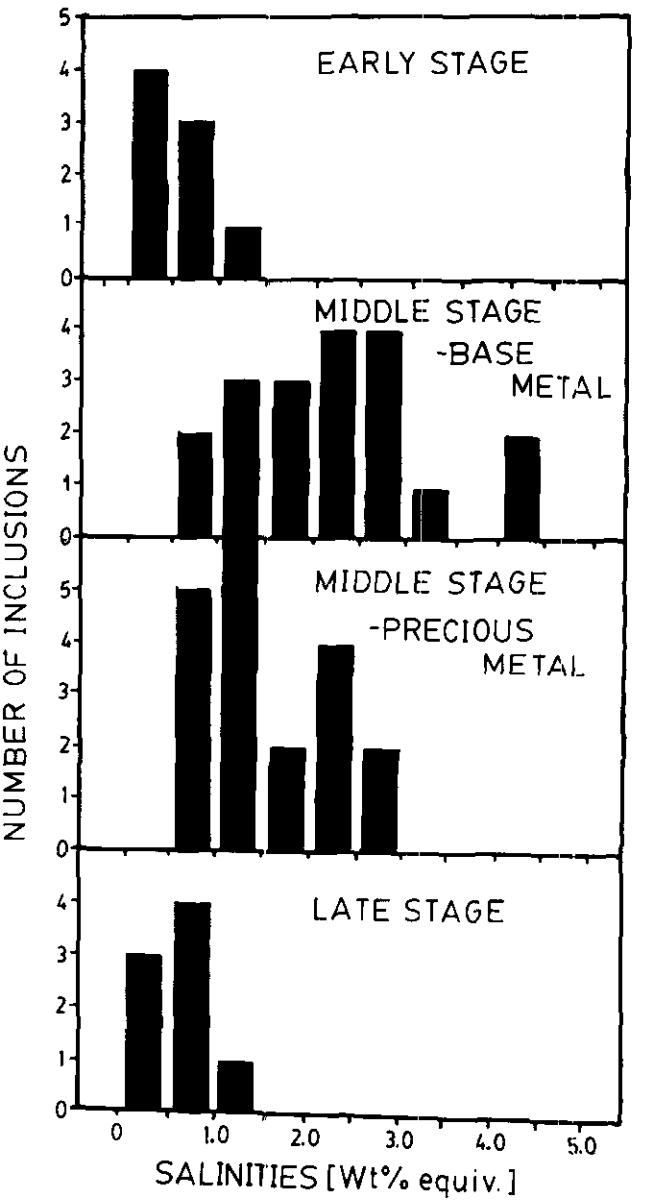

Figure 2-12-5. Histogram of salinity for primary fluid inclusions from all stages of veining.

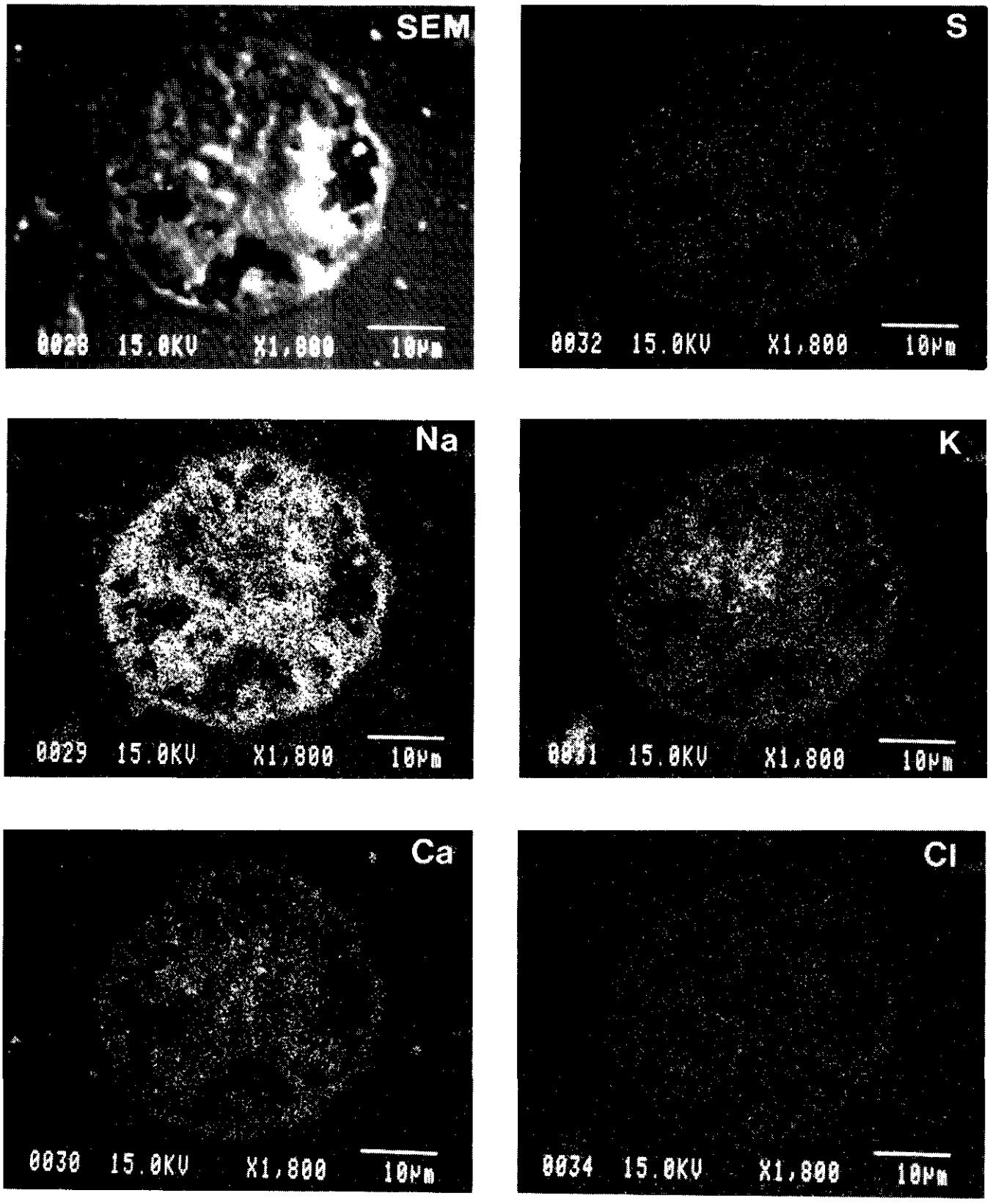

Plate 2-12-2. SEM photomicrograph of a decrepitation precipitate from a precious metal-rich, middle-stage vein. Sample SP-214-A. X-ray dot maps with the EDS system for S, Na, K, Ca, Cl.

molar proportions. A CO_2 peak from Sample SP-14, a base metal rich, middle-stage vein has the following values:

$A_{(CO2)} = 97$;

$\Sigma A = 229\ 534$;

$\sigma_i = 1.21$ (Schrotter and Klockner, 1979).

The instrument correction factors are not required because the Raman spectrometer has a multidiode array. Thus:

$$Xi = (A_{CO2}/\sigma_i f_i)/(\Sigma A_i/\sigma_i f_i),$$
$$= (97/1.21)/(229{,}534/1.21)$$
$$= 4.22 \times 10^{-4} \text{ moles.}$$

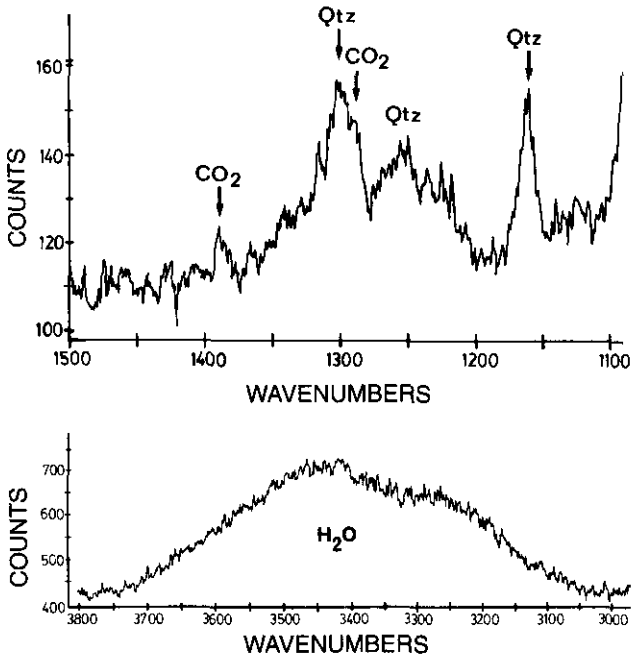

Figure 2-12-6. Raman spectra of middle-stage, sulphide-bearing veins.

A. The presence of minor CO_2 in a H_2O-dominant inclusion. CO_2 peaks are at 1292 and 1387 cm^{-1}. Sample number SP-14.

B. Pure H_2O inclusion in quartz. The small, narrow peaks are extremely weak and have not been identified. Both spectra are from a multichannel scan, 10 points per second, points spaced 0.3 cm^{-1}. Sample number SP-50-S.

TABLE 2-12-3
LASER RAMAN MICROSCOPE – SPECIES OF GASES

	GAS SPECIES – VOLUME %						
	SO_2	CO_2	CO	N_2	H_2S	CH_4	H_2O
EARLY-STAGE	N.D.	N.D.	N.D.	N.D.	N.D.	N.D.	<99
MIDDLE-STAGE							
PRECIOUS METAL RICH	N.D.	<1	N.D.	TRACE	N.D.	N.D.	99
BASE METAL RICH	N.D.	1-2	TRACE	TRACE	N.D.	N.D.	98
LATE-STAGE	N.D.	N.D.	N.D.	N.D.	N.D.	N.D.	99

* N.D. – Not detected.

Therefore the CO_2 mole fraction in a precious metal rich middle-stage vein is 4.22×10^{-4}. This low CO_2 abundance should have little affect on pressure corrections of homogenization temperatures and depth determinations. Salts such as NaCl, KCl and $CaCl_2$ are not appreciably Raman-active either in pure crystalline form or in aqueous solution, so electron microprobe analysis of fluid inclusion precipitates has been attempted.

ELECTRON MICROPROBE

After heating and freezing temperatures have been measured, the temperature of the heating stage is raised at a rate of 15° to 20°C per minute to 570°C. The inclusion is ruptured and the decrepitating fluid forms a precipitate on the surface of the slide. The decrepitation precipitates generally have a yellowish brown colour and a shape similar to that of a volcanic crater (Plate 2-12-2).

Semiquantitative analysis of individual fluid inclusions can be obtained by analyzing the precipitates, which are the bulk of the nonvolatile compounds in the inclusion. The Jeol JXA-8600 electron microprobe, in the energy dispersive mode (EDS) with an accelerating voltage of 15 kilovolts has been used for scan analysis of the decrepitation precipitates (Table 2-12-3).

A scanning microscope was used to define the chemical constituents within the precipitates using a conventional x-ray dot map in scanning mode (Plate 2-12-2). For all stages of veining, sodium, calcium and sulphur scans have the most intense patterns with dispersed patterns for potassium, chlorine and manganese. Both early and late-stage veins, have no concentrations of chlorine, manganese and fluorine. In both base and precious metal rich veins, silver precipitate is defined by electron backscatter and intense x-ray maps (Plate 2-12-3).

VERTICAL THERMAL GRADIENTS

Homogenization temperatures of quartz in middle-stage veins and breccias are contoured as 210°, 220°, and 230°C isotherms and superimposed on a longitudinal section of Silbak Premier mine workings (Figure 2-12-7). These isotherms define a broad thermal gradient that parallels the plunge of mineralized zones. There is a systematic decrease in temperature with depth, however, there is a low-temperature zone between 5 and 6-level. Homogenization temperatures have a greater variation lower in the deposit.

PRESSURE CORRECTIONS AND PALEODEPTH ESTIMATES

Where hydrothermal fluids have not been boiled, fluid inclusion homogenization temperatures require a pressure correction to obtain the trapping temperature. Most inclusions have trapped fluids at a pressure-temperature combination above the liquid/vapour curve (Figure 2-12-8). A bubble does not occur in the inclusion until the pressure and temperature have dropped to the liquid/vapour curve. Because an inclusion has a constant density, the cooling path follows an isochore corresponding to its density.

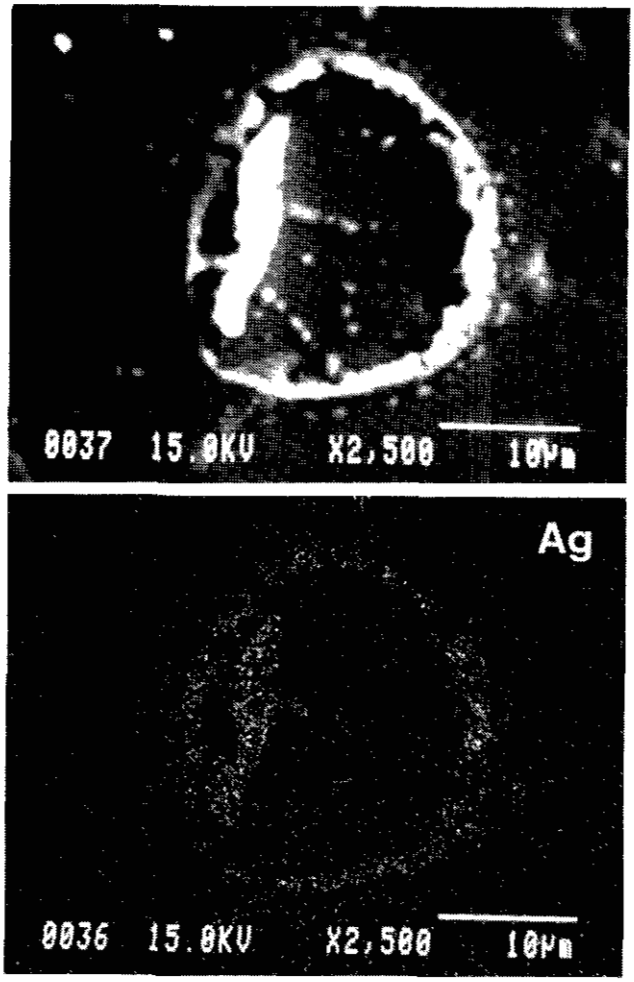

Plate 2-12-3A. Decrepitation precipitate of a precious metal rich, middle-stage vein in the backscatter electron scanning mode (A). Sample SP-47-U. The backscatter image provides a map of the spatial variation of average atomic number. Silver has an intense white backscatter image. B. X-ray dot map of silver in the precipitate.

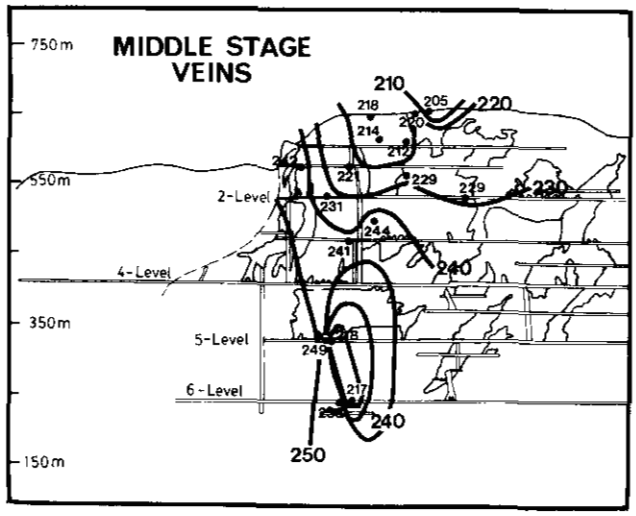

Figure 2-12-7. Longitudinal section, parallel to the Main zone trend (Figure 2-12-2) of the Silbak Premier mine workings (Grove, 1971). Shaded areas are shrinkage stopes. Contoured homogenization temperature isotherms of fluid inclusions, from both precious and base metal, middle-stage veins, are superimposed on the section. Isotherms are skewed updip parallel to the stopes.

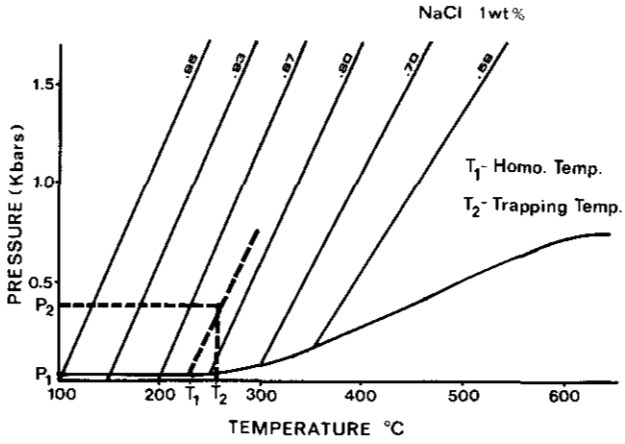

Figure 2-12-8. P-T section for 1 weight per cent NaCl aqueous solution. Density (g/cm^3) of aqueous NaCl solutions contoured on pressure-temperature (P-T) coordinates. Isochores are lines of constant volume and hence constant density. The degree of filling indicates the density of the ore-forming fluid is 0.83 (Roedder and Bodnar, 1980).

In the case of homogenization by disappearance of vapour bubbles, the minimum pressure is read directly from the corresponding isopethal PT section of the H_2O-NaCl system (Figure 2-12-8). Using the intersecting-isochore method, a trapping temperature of 226°C (T_1) has a pressure (P_1) of less than 10 bars. An independent pressure estimate, using degree of fill and temperature (Roedder and Bodnar, 1980) indicates a true confining pressure (P_2) of 35,000 kilopascals (350 bars). Consequently, the pressure-corrected trapping temperature (T_2) is 255°C for middle-stage base metal rich veins. Trapping temperatures for other stages of veining are given in Table 2-12-4.

Identification of even small amounts of dissolved gas such as CO_2, CO, N_2, H_2S and CH_4 in inclusions can significantly affect the pressure estimates (Pasteris *et al.*, 1986). The addition of even small amounts of CO_2 to H_2O-NaCl significantly raises the vapour pressure and concomitantly, the calculated depth of formation. Because inclusions are H_2O-dominant in all stages of veining, with only trace amounts of

TABLE 2-12-4
CONVERSION OF PRIMARY HOMOGENIZATION TEMPERATURES TO TRAPPING TEMPERATURES.

	HOMOGENIZATION TEMPERATURE °C	TRAPPING TEMPERATURE °C
EARLY-STAGE VEINS	204.6	239.8
MIDDLE-STAGE VEINS:		
PRECIOUS METAL RICH	225.4	256.3
BASE METAL RICH	228.81	258.2
LATE-STAGE VEINS	208.5	234.1

CO_2, N_2 and CO, temperature and pressure corrections are small.

Paleodepth estimates determined from fluid inclusions are based on the pressure-temperature-salinity relationships (Haas, 1971) and related to a maximum depth for an incipient boiling NaCl brine. The temperature-pressure-salinity data from Silbak Premier indicate a fluid pressure corresponding to a depth of 600 metres in a slightly saline fluid. Estimates determined by this method can have large uncertainties because of the presence of water vapour bubbles, carbon dioxide and other gases and changing hydrostatic versus lithostatic load conditions.

INTERPRETATION

Self-sealing and rebreaking of hydrothermal breccias in active geothermal systems is well described from several locations (Henley, 1985). The wide range of homogenization temperatures of primary inclusions in quartz may reflect a continuum of several hydrothermal episodes rather than one specific event. Many of the quartz veins examined in this study are repeatedly fractured by recurrent movements of the veins, resulting in abundant planes of pseudosecondary and secondary inclusions.

Fluid inclusions in early-stage veins have low homogenization temperatures and salinities and are spacially and temporally associated with intrusive porphyritic dacite. There is a significant increase in homogenization temperatures and salinities associated with base and precious metal deposition. Late-stage veins are produced in extension zones during the waning stages of hydrothermal activity.

The inclusions are aqueous and have dissolved sulphur, sodium, calcium, potassium, manganese and ore metals, such as copper and silver, which form in the decrepitation precipitates. Large concentrations of sulphur in calcium-rich fluid inclusions suggest the fluids may have provided the necessary sulphur to precipitate silver as a sulphide or sulphosalt.

The mixing of meteoric waters with hot, metal-bearing fluids, is the most likely mechanism for base and precious metal deposition, because there is no coexistance of liquid-rich and vapour-rich inclusions to indicate boiling. Decreasing temperature, and increasing pH with mixing, causes bisulphide complexes to release metals and precipitate sulphide minerals (Spycher and Reed, 1989). Aqueous sulphide may be sufficiently depleted by sulphide precipitation to cause gold to precipitate from $Au(HS)^{-2}$.

Reaction with the wallrocks could have changed the pH or decreased the H_2S activity of fluids, but this is likely to have affected the vein system evenly, resulting in widespread gold in wallrock rather than the observed spotty deposition of high-grade ore shoots. The restriction of high-grade ore to late fractures in the veins also suggests that the ore-forming fluid had limited interaction with the wallrock.

In contrast, separation of the ore fluid into immiscible phases, accompanied by the escape of CO_2 vapour, is more localized and abrupt and may have formed much of the vein ore. These effects contribute to the "telescoping" or vertical changes in base and precious metal abundances in epithermal deposits. The same effects could also produce sulphide-rich, precious metal-rich and barren stages in ore formation.

If salinity is relatively uniform, vertical gradients in T_h indicate density gradients and hence the direction of fluid movement (Roedder, 1984). The change from base to precious metal rich assemblages and declining sulphide abundances coincide with temperature decreases. Declining temperatures in the lower part of the deposit may also indicate a bottoming of the hydrothermal system. Unfortunately, not enough fluid inclusion data are available to determine if there is a correlation between the variation in the ore grade and the composition of the associated inclusions.

The temperatures and salinities of base and precious metal vein stages at Silbak Premier are reminiscent of adularia-sericite epithermal deposits (Heald *et al.*, 1987), but in contrast have large proportions of base metals and spatial association with intrusions. The Silbak Premier deposit has common characteristics with silver-gold deposits in the Iskut and Unuk River valleys and may represent a distinct epithermal metallogenic district.

APPLICATION IN EXPLORATION

With increasing sophistication of analytical techniques and availability of fluid inclusion data, the quantitative chemical evolution over a range of depths can be used as a guide to ore and provide a way of comparing ore deposit models. Because halos of fluid inclusions are more widespread than correponding halos of alteration minerals (Bodnar, 1981), they are larger targets for mineral exploration provided appropriate techniques are used. Homogenization temperatures of fluid inclusions in hydrothermal systems increase as new inclusions form closer to the ore (Roedder, 1984). Reconstruction of isotherms may therefore hold promise as an exploration tool in similar silver-gold vein deposits. Increasing concentrations of salt, carbon dioxide and other gases also indicate proximity to mineral occurrences.

CONCLUSIONS

The incorporation of fluid inclusion data with surface and underground mapping leads to the following geologic reconstruction of the Silbak Premier orebodies:

(1) Conjugate fault sets are the locus of a series of porphyritic dacite intrusions into andesite flows, breccias and tuffs. Hydrothermal fluids followed emplacement of porphyritic dacite, initially into diffuse areas of crackle breccia along the margins of the dacite, subsequently into crosscutting conjugate fault sets. Base and precious metal precipitates along these faults were sucessively sealed and broken. Fluids barren of metal and sulphur were emplaced along tensional features in the last stage of the hydrothermal event.

(2) The close proximity, in both time and space, of the Texas Creek granodiorite to porphyritic dacite and metal-bearing veins and breccias suggests a partial magmatic source for heat, fluids and metals. These magmatic fluids may mix with meteoric water or, to a lesser extent seawater.

(3) Vein-hosted base and precious metals were deposited at pressure-corrected temperatures of 250° to 260°C at a minimum depth of 500 metres. Typically, these veins formed in hydrous fluids with salinities less than 4.5

equivalent weight per cent NaCl. A limited number of inclusions contain liquid carbon dioxide, with lesser nitrogen and carbon monoxide gas. Sodium, calcium, sulphur and silver are the dominant dissolved constituents with lesser amounts of chlorine, potassium, manganese, iron and magnesium. Metal transport and deposition in hydrothermal fluids coincided with thermal peaks and fluids of greatest salinity. Both early and late-stage veins have lower temperatures and salinities.

(4) Where low-temperature hydrothermal fluids have elevated sulphur concentrations, thiosulphides are the dominant complexing agent. The mixing of magmatic, H_2S-rich hydrothermal fluids with meteoric waters decreases temperatures and increases pH and oxygen content of the hydrothermal fluids causing bisulphide complexes to precipitate sulphides, sulphosalts and finally native metals. Restricted lateral distribution and changes from barren to base metal rich, then precious metal rich assemblages with elevation, coincide with a moderating thermal and salinity gradients. These gradients, in combination with declining sulphide abundances, reflect the declining solubilities first of base metals then of precious metals.

ACKNOWLEDGMENTS

This study represents part of a Ph.D. thesis in progress at the University of Western Ontario. Field support was generously provided by Westmin Resources Limited and thanks are due to H. Meade, P.Wodjak and A. Randall for their cooperation. Additional funding was provided by a British Columbia Geoscience Research Grant Number RG89-07 and a Hirshhorn Scholarship at the University of Western Ontario. The author has benefited from numerous discussions and gratefully acknowledges R.W. Hodder, S. Chrysoulis and D. Marshall. Special thanks to D. Kingston for helping re-establish the fluid inclusion lab at Western and for guidance on the microprobe. I. Hill at Surface Science Western operated the laser Raman spectrometer and J. Forth prepared the doubly polished thin sections.

REFERENCES

Alldrick, D.J. (1985): Stratigraphy and Petrology of the Stewart Mining Camp (104B/1); *B.C. Ministry of Energy, Mines and Petroleum Resources*, Geological Fieldwork 1984, Paper 1985-1, pages 316-341.

——— (1987): Geology and Mineral Deposits of the Salmon River Valley, Stewart Area (NTS 104A, B); 1:50 000 scale; *B.C. Ministry of Energy, Mines and Petroleum Resources*, Open File 1987-22.

Alldrick, D.J., Brown, D.A., Harakal, J.K. and Armstrong, R.L. (1987): Geochronology of the Stewart Mining Camp (104B/1); *B.C. Ministry of Energy, Mines and Petroleum Resources*, Geological Fieldwork 1986, Paper 1987-1, pages 81-92.

Bodnar, R.J. (1981): Use of Fluid Inclusions in Mineral Exploration: Comparison of Observed Features Theoretical and Experimental Data on Ore Genesis; *Geological Society of America*, Abstract Programs, Volume 13, page 412.

Brown, D. (1987): Geological Setting of the Volcanic-hosted Silbak-Premier Mine, Northwestern B.C. (NTS 104A/4, 104B/1); unpublished M.Sc. thesis, *The University of British Columbia*, 216 pages.

Delhaye, M. and Dhamelincourt, P. (1975): Raman Microprobe and Microscope with Laser Excitation; *Journal Raman Spectroscopy*, Volume 3, pages 33-38.

Grove, E.W. (1971): Geology and Mineral Deposits of the Stewart Area, Northwestern British Columbia; *B.C. Ministry Energy, Mines and Petroleum Resources*, Bulletin 58, 229 pages.

Haas, J.L., Jr. (1971): The Effect of Salinity on the Maximum Thermal Gradient of a Hydrothermal System at Hydrostatic Pressure; *Economic Geology*, Volume 66, pages 940-946.

Heald, P., Foley, N.K. and Hayba, D.O. (1987): Comparative Anatomy of Volcanic-hosted Epithermal Deposits: Acid-sulphate and Adularia-sericite Types; *Economic Geology*, Volume 82, pages 1-26.

Henley, R.D. (1985): The Geothermal Framework of Epithermal Deposits, *in* Geology and Geochemistry of Epithermal Systems; Berger, B.R. and Bethke, P.M., Editors, *Society of Economic Geologists*, Reviews in Economic Geology, Volume 2, pages 1-24.

MacDonald, A.J. and Spooner, E.T.C. (1981): Calibration of a Linkam TH 600 Programmable Heating-cooling Stage for Microthermometric Examination of Fluid Inclusions; *Economic Geology*, Volume 76, pages 1248-1258.

McDonald, D.W. (1988): Metallic Minerals in the Silbak Premier Silver-gold Deposit; *B.C. Ministry of Energy, Mines and Petroleum Resources*, Geological Fieldwork 1987, Paper 1988-1, pages 349-352.

Pasteris, J.D., Kuehn, C.A. and Bodnar, R.J. (1986): Applications of the Laser Raman Microprobe RAMANOR U-1000 to Hydrothermal Ore Deposits: Carlin as an Example; *Economic Geology*, Volume 81, pages 915-930.

Randall, A.W. (1988): Geological Setting and Mineralization of the Silbak Premier and Big Missouri Deposits; *in* Field Guide Book; Major Gold-silver Deposits of the Northern Canadian Cordillera, *Society of Economic Geologists*, pages 85-99.

Roedder, E. (1984): Fluid Inclusions, *in* Reviews in Geology; Volume 12; *Mineralogical Society of America*, 646 pages.

Roedder, E. and Bodnar, R.J. (1980): Geologic Pressure Determinations from Fluid Inclusion Studies; *Annual Review Earth Planetary Science*, Volume 8, pages 263-301.

Rosasco, G.J., Roedder, E. and Simmons, J.H. (1975): Laser-excited Raman Spectrometer for Nondestructive Analysis of Sulfate in Individual Phases in Fluid Inclusions in Minerals; *Science*, Volume 190, pages 557-560.

Schrotter, H.W. and Klockner, H.W. (1979): Raman Scattering Cross-sections in Gases and Liquids, *in* Raman Spectrometry of Gases and Liquids, A. Weber, Editor, pages 123-166.

Spycher, N.F. and Reed, M.H. (1989): Evolution of a Broadlands-type Epithermal Ore Fluid along Alternative P-T Paths: Implications for the Transport and Deposition of Base, Precious, and Volatile Metals; *Economic Geology*, Volume 84, pages 328-359.

Wopenka, B. and Pasteris, J.D. (1986): Limitations to Quantitative Analysis of Fluid Inclusions in Geological Samples by Laser Raman Microprobe Spectrometry; *Applied Spectrometry*, Volume 40, pages 144-151.

——— (1987): Raman Intensities and Detection Limits of Geochemically Relevant Gas Mixtures for a Laser Raman Microprobe; *Analytical Chemistry*, Volume 59, pages 2165-2170.

NOTES